Asociación Argentina
de Mecánica Computacional

Mecánica Computacional Vol XXIX, págs. 5961-5971 (artículo completo)
Eduardo Dvorkin, Marcela Goldschmit, Mario Storti (Eds.)
Buenos Aires, Argentina, 15-18 Noviembre 2010

COMPARING ABSORBING BOUNDARY CONDITIONS FOR A 3D NON NEWTONIAN FLUID-STRUCTURE INTERACTION MODEL FOR BLOOD FLOW IN ARTERIES

João Janela[c,b], **Alexandra B. de Moura**[a,b] **and Adélia Sequeira**[a,b]

[a]*Department of Mathematics, Instituto Superior Técnico, Av. Rovisco Pais, 1, 1049-001, Lisboa, Portugal, alexandra.moura@math.ist.utl.pt, http://www.ist.utl.pt*

[b]*CEMAT-Center for Mathematics and its Applications, Instituto Superior Técnico, Av. Rovisco Pais, 1, 1049-001, Lisboa, Portugal, http://cemat.ist.utl.pt*

[c]*Department of Mathematics, Instituto Superior de Economia e Gestão, Rua do Quelhas, 6, 1200-781, Lisboa, https://aquila.iseg.utl.pt/aquila/instituicao/ISEG*

Keywords: Fluid-structure interaction (FSI), Absorbing boundary conditions, Non-Newtonian fluid, 1D model, Blood flow

Abstract. A 3D fluid-structure interaction (FSI) problem in a compliant vessel, consisting of a hyper-elastic structure model coupled with a shear-thinning generalized Newtonian fluid, is used to represent the pressure wave propagation that characterizes blood flow in arteries, and several absorbing boundary conditions are analyzed in order to avoid the numerical spurious reflections due to the truncation of the domain. First, the 3D FSI model is coupled to a 1D hyperbolic model that captures very well the pulse propagation nature of blood flow in arteries. This coupling has been shown to be stable at the continuous level, and the 1D model proved to effectively absorb the pressure wave outgoing the 3D domain. Afterward, other absorbing boundary conditions, based on a simple analysis of the characteristics of the 1D hyperbolic model, are imposed directly on the outflow sections of the 3D FSI problem. These conditions, which can be identified with linear resistance models, relate the mean pressure with the volume flow rate at the artificial section at hand. Numerical results comparing the 3D-1D coupling and the different absorbing conditions in both idealized and realistic geometries, reconstructed from medical imaging, are discussed.

1 INTRODUCTION

Mathematical modeling and numerical simulation of the human cardiovascular system are nowadays very important tools in understanding the genesis and development of cardiovascular diseases, which are one of the leading causes of death in developed countries. However, this is a difficult task due to the geometrical and functional complexity of the vascular system (Formaggia et al., 2009). On one hand, detailed 3D information on the blood flow field in patient-specific geometries, is required to understand cardiovascular pathologies. On the other hand, realistic simulations of blood flow in arteries cannot be performed in extensive 3D regions, due to its geometrical complexity and computational cost. However, the arterial system is closed, and the truncation of the physical domain should be performed without loosing information on the flow behavior in the systemic circulation. Moreover, blood is a non-Newtonian fluid interacting with the artery wall, that moves under the blood load, giving rise to propagating pressure waves that characterize blood flow in arteries (Formaggia et al., 2009).

Blood is a concentrated suspension of red blood cells (RBC), white blood cells, and platelets in plasma, having a complex rheological behavior. One of the main non-Newtonian properties of blood is its shear-thinning behavior, which is largely explained by the RBCs ability to aggregate into 3D microstructures (*rouleaux*) at low shear rates, and their tendency to align with the flow field at high shear rates (Chien et al., 1970; Robertson et al., 2008; Formaggia et al., 2009). In this work blood is considered as an inelastic shear-thinning fluid, modeled by the Carreau non-Newtonian law for the viscosity, fitted to experimental data (Janela et al., 2010b).

The vascular wall is an inhomogeneous multi-layer nonlinear material, which deforms under the action of blood flow. It is a very complex structure and *in vivo* data are difficult to obtain, so that the devision of appropriate constitutive laws is still an open problem. For this reason, many studies of the hemodynamics in arteries are carried out in rigid domains, without taking into account the motion of the artery wall. Here, following previous works (Fernández and Moubachir, 2005; Formaggia et al., 2007; Janela et al., 2010a,b; Formaggia et al., 2009), the artery wall is modeled as a nearly incompressible 3D hyperelastic material.

The mathematical and numerical analysis of the highly non-linear FSI problem is still a field of active research, and FSI problems with non-Newtonian blood models are practically not addressed in literature. Recent contributions can be found in Janela et al. (2010a,b). In this study a fully implicit partitioned numerical method (see Fernández and Moubachir, 2005) is used, consisting in solving the FSI coupling by iterating the fluid and structure sub-problems, supplied with suitable (Dirichlet to Neumann) matching conditions.

The complexity and computational cost of 3D FSI simulations make it necessary to truncate the computational domain of interest, originating the so-called artificial boundary sections. In order to accurately represent the wave propagation phenomena, absorbing boundary conditions should be considered in the outflow artificial boundaries, so that spurious reflections due to the truncation of the domain are avoided. In the present work several types of artificial boundary conditions are taken into account and compared. First, the 3D FSI non-Newtonian problem is coupled to a 1D hyperbolic model (Formaggia et al., 2007; Janela et al., 2010b), obtained from the 3D FSI model by making simplifying assumptions and averaging over the cross section of the artery (Formaggia and Veneziani, 2003). The 1D model captures very well the wave propagation of blood flow in arteries, and coupled to the 3D FSI model effectively acts as absorbing boundary condition (Janela et al., 2010b; Formaggia et al., 2007). Moreover, 1D models can represent large arterial trees (Alastruey et al., 2007) and be coupled both at the inflow and outflow of the 3D FSI model (Moura, 2007), so that the 3D model can be embedded

into large 1D networks. Secondly, absorbing boundary conditions obtained from the 1D model are devised and imposed directly into the 3D FSI problem (Janela et al., 2010b). These are derived by canceling the 1D incoming characteristic, obtaining a non linear condition between flow rate and mean pressure. A linear absorbing boundary condition, that can be identified with a resistance model, is also derived.

The several boundary conditions are compared in a cylindrical tube, and also applied to an anatomically realistic geometry of a carotid bifurcation. Numerical results demonstrate the efficiency of the conditions proposed to absorb outgoing pressure waves of the 3D domain, predicting its future application to hemodynamic simulations in compliant vessels.

2 THE 3D NON-NEWTONIAN FSI MODEL

In this study blood is modeled as an incompressible Carreau generalized Newtonian fluid, governed by the following momentum and continuity equations, written in Eulerian coordinates:

$$\left\{ \begin{array}{rcll} \rho\left(\dfrac{\partial \mathbf{u}}{\partial t} + \mathbf{u}\cdot\nabla\mathbf{u}\right) + \nabla p - \operatorname{div}\left(\mu(\dot\gamma)(\nabla\mathbf{u} + \nabla\mathbf{u}^T)\right) & = & \mathbf{0}, & \text{in } \Omega^t, \forall t \in I \\ \operatorname{div}\mathbf{u} & = & 0, & \text{in } \Omega^t, \forall t \in I \end{array} \right. \tag{1}$$

for the time interval $I =]0, T]$, with $T > 0$. These equations will be coupled with a structure model, and the domain where they are defined will change in time. The reference domain is denoted by Ω^0, while Ω^t is the current domain, with $t \in I$. In (1) ρ is the constant fluid density, $\mathbf{u}$ and p are the fluid unknown velocity and pressure, μ is the shear dependent viscosity, and $\dot\gamma = \sqrt{\frac{1}{2}(\nabla\mathbf{u} + \nabla\mathbf{u}^T) : (\nabla\mathbf{u} + \nabla\mathbf{u}^T)}$ is the shear rate. The Carreau viscosity function is given by:

$$\mu(\dot\gamma) = \mu_\infty + (\mu_0 - \mu_\infty)(1 + (\lambda\dot\gamma)^2)^{(n-1)/2},$$

where parameters $\mu_0, \mu_\infty, \lambda$, and n are obtained by fitting experimental data. The experimental viscosity data used were obtained by Prof. M.V. Kameneva (Univ. Pittsburgh) as described in Janela et al. (2010b), obtaining $\mu_0 = 0.456\ Poi$, $\mu_\infty = 0.032\ Poi$, $\lambda = 10.03$, and $n = 0.344$. In Figure 1 is plotted the Carreau viscosity function with these parameters.

As initial condition we take $\mathbf{u} = \mathbf{u}_0$ in Ω^0. The boundary condition on the physical wall, denoted Γ_w^t, will be given by the coupling with the structure model. On the artificial sections, the boundary conditions must account for the remaining parts of the system. For this matter, first reduced 1D models will be coupled to the 3D, afterward proper absorbing conditions will be set up.

The vessel wall is assumed to be a 3D compressible elastic material. It is defined in the 3D solid domain, varying in time, and denoted as Σ^t, being Σ^0 its reference configuration. The equations are given, in Lagrangian coordinates, by (see Ciarlet, 2004):

$$\rho_w \frac{\partial^2 \boldsymbol{\eta}}{\partial t^2} - \operatorname{div}_0(\mathbf{P}) = \mathbf{0}, \quad \text{in } \Sigma^0, \forall t \in I, \tag{2}$$

where $\boldsymbol{\eta}$ is the unknown displacement vector, ρ_w is the wall density, div_0 is the divergence operator with respect to the Lagrangian coordinates, and $\mathbf{P}$ is the first Piola-Kirchhoff tensor.

We consider a St Venant-Kirchhoff material (Ciarlet, 2004, Section 3.9), for which the response function for the second Piola-Kirchhoff tensor is linear as a function of the Green - St Venant strain tensor $\mathbf{e} = \frac{1}{2}\left(\nabla_0^T\boldsymbol{\eta} + \nabla_0\boldsymbol{\eta}\right)$: $\mathbf{S} = \lambda\operatorname{tr}(\mathbf{e})\mathbf{I} + 2\mu\mathbf{e}$, with $\lambda = \frac{E\xi}{(1+\xi)(1-2\xi)}$ and

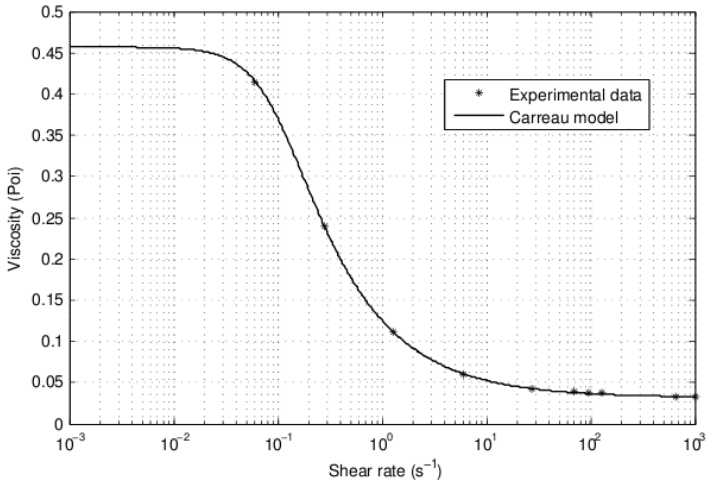

Figure 1: Apparent viscosity as a function of shear rate for the Carreau model.

$\mu = \frac{E}{2(1+\xi)}$ the Lamé constants, being E the Young modulus and ξ the Poisson ratio. In this study we consider a nearly incompressible material by setting a Poisson ratio close to 0.5 and a constant mass density ρ_w.

The initial condition for (2) is set to be $\boldsymbol{\eta} = \boldsymbol{\eta}_0$, and $\dot{\boldsymbol{\eta}} = \dot{\boldsymbol{\eta}}_0$ in Σ^0, verifying the compatibility constraint $\dot{\boldsymbol{\eta}}_0 = \mathbf{u}_0$, on Γ_w^t. At the exterior boundary we assume that the stress is zero.

At the interface with the fluid Γ_w^0, the boundary condition is given by the fluid-structure interaction (FSI) coupling, which is performed through the following matching conditions:

$$\mathbf{u} = \dot{\boldsymbol{\eta}}, \quad \forall t \in I, \text{ on } \Gamma_w^t, \tag{3}$$

$$-\left(\det \nabla_{\mathbf{0}} \boldsymbol{\eta}\right) \boldsymbol{\sigma}(\mathbf{u}, P) \left(\nabla_{\mathbf{0}}{}^{-T} \boldsymbol{\eta}\right) \cdot \mathbf{n}_0 = \mathbf{P}(\boldsymbol{\eta}) \cdot \mathbf{n}_0, \quad \forall t \in I, \text{ on } \Gamma_w^0, \tag{4}$$

where $\nabla_{\mathbf{0}}$ indicates the gradient with respect to the Lagrangian coordinates, and $\mathbf{n}_0$ is the outward unit vector to Γ_w^0. The first is the no-slip conditions and it is imposed on the fluid model, thus being written in Eulerian coordinates, while the later establishes the continuity of the normal stresses and it is imposed on the solid model, thus being written in the Lagrangian frame through the Piola transform.

An energy estimate for this 3D FSI non-Newtonian coupling has been demonstrated in Janela et al. (2010a).

3 ABSORBING BOUNDARY CONDITONS

In this Section we focus on the prescription of boundary conditions at the artificial sections of the 3D FSI non-Newtonian problem previously introduced. We will mainly discuss absorbing boundary conditions, which are essential at outflow sections. These are typically at the downstream (closer to systemic circulation). Nevertheless, since blood flow in arteries is pulsatile, due to the action of the heart and the compliance of the vessels, downstream sections can experience incoming flow. Notice that the techniques presented in the sequel can be applied at both inflow or outflow sections, whence, at both upstream (closer to the heart) or downstream boundaries. For the sake of simplicity, and without loss of generality, a prescribed inflow velocity or pressure (normal stress) is considered at the inflow upstream section, while the presented absorbing conditions will be taken at the outflow boundary.

3.1 The 1D model

The 1D model is derived from the 3D FSI model by making simplifying assumptions and integrating over the artery cross section (Formaggia and Veneziani, 2003). Assuming a flat velocity profile, the 1D model for blood flow in a cylindrical vessel is given by the following system of PDEs:

$$\begin{cases} \dfrac{\partial A}{\partial t} + \dfrac{\partial Q}{\partial z} = 0, \\ \dfrac{\partial Q}{\partial t} + \dfrac{\partial}{\partial z}\left(\dfrac{Q^2}{A}\right) + \dfrac{A}{\rho}\dfrac{\partial \overline{p}}{\partial z} = -K_r \dfrac{Q}{A}, \end{cases} \quad \forall t \in I, \tag{5}$$

where z is the axial coordinate, ρ is the constant fluid density, K_r is the friction coefficient and it is defined by $K_r = 8\pi\nu$, with ν the blood dynamic viscosity. In this work the 1D model does not account for the shear-thinning behavior of blood, being the viscosity ν constant.

The unknowns are the cross-section area $A(z)$, the flow rate $Q(z)$, and the mean pressure $\overline{p}(z)$. We endow system (5) with the simple pressure-area algebraic relation (Formaggia and Veneziani, 2003; Formaggia et al., 2007, 2009):

$$\overline{p} = \beta \frac{\sqrt{A} - \sqrt{A_0}}{A_0}, \quad \text{with} \quad \beta = \frac{\sqrt{\pi} h_0 E}{1 - \xi^2}, \tag{6}$$

with A_0 the cross-section reference area at rest, E the Young modulus, h_0 the wall thickness, and ξ the Poisson ratio. Both A_0 and β may vary along the vessel length z.

System (5) with (6) is hyperbolic, having two distinct eigenvalues $\lambda_{1,2} = \overline{u} \pm \sqrt{\frac{\beta}{2\rho A_0}} A^{\frac{1}{4}}$, with $\overline{u} = \frac{Q}{A}$ the mean velocity. Under physiological conditions in hemodynamics, the eigenvalues $\lambda_{1,2}$ have opposite signs, *i.e.* the flow is sub-critical (see Formaggia and Veneziani, 2003). Their corresponding eigenfunctions or characteristic variables are:

$$W_{1,2}(Q, A) = \overline{u} \pm 4\sqrt{\frac{\beta}{2\rho A_0}} \left(A^{\frac{1}{4}} - A_0^{\frac{1}{4}}\right), \tag{7}$$

being W_1 the incoming characteristic at the left extremity (inflow) of the vessel, and W_2 the incoming characteristic at the right extremity (outflow) of the vessel.

System (5)-(6) is provided with initial, $A(0, \cdot) = A^0(\cdot)$, and $Q(0, \cdot) = Q^0(\cdot)$, and boundary conditions, $W_1(t) = g_1(t)$, at the left extremity, and $W_2(t) = g_2(t)$, at the right extremity.

3.2 Coupling with the 1D model

In order to prescribe adequate boundary conditions, the 3D outflow section is coupled to a 1D model, that can represent a singular cylinder or a network of arteries. The coupling is performed imposing the continuity of the normal stresses and the fluxes:

$$p\mathbf{n} - 2\mu(\dot{\gamma})\mathbf{D}(\mathbf{u}) \cdot \mathbf{n} = \left(\overline{p}_{1D} + \frac{\rho}{2}|\overline{u}_{1D}|^2\right)\mathbf{n}, \tag{8}$$

$$Q_{3D} = \int_{\Gamma_a^t} \mathbf{u} \cdot \mathbf{n} d\gamma = Q_{1D}. \tag{9}$$

In Janela et al. (2010b) an energy estimate is derived for this 3D FSI non-Newtonian - 1D coupling. There the authors reformulate the Navier-Stokes equations (1) obtaining a different

matching condition (8), establishing the continuity of the total normal stresses instead of the normal stresses. As discussed in Formaggia et al. (2007), and Janela et al. (2010b, Remark 5.2), although the reformulation of the Navier-Stokes equations proposed in Janela et al. (2010b) is essential to obtain the stability result, in hemodynamics the term $\frac{\rho}{2}|\mathbf{u}|^2$ is negligible compared to the pressure values. This means that in practice, for blood flow simulations, the standard Navier-Stokes formulation considered in this study works equally well with condition (8) when coupled to the 1D model.

The 3D-1D coupling can be performed imposing (8) into the 3D problem, and (9) into the 1D model, or *vice-versa*. We consider the former approach (Janela et al., 2010b): the total pressure computed on the 1D model is provided to the 3D model through a constant Neumann boundary condition (Heywood et al., 1996), while the flow rate computed on the 3D artificial section is prescribed at the 1D inflow boundary.

At the right extremity of the 1D model the incoming characteristic is set to zero, $W_2(Q, \bar{p}) = 0$, so that only the exiting characteristic remains, eliminating the spurious reflections that might enter the domain. In this way, an absorbing boundary condition is prescribed at the 1D outflow boundary.

A staggered numerical algorithm is used, consisting of an iterative procedure between the 3D FSI and 1D subproblems. This iterative scheme can be considered explicit or implicit (Moura, 2007). Numerical tests already performed (see Formaggia et al., 2007; Moura, 2007) in the Newtonian case show that, as long as the continuity of the area is not forced at the 3D-1D coupling interface, the explicit scheme remains stable. Whenever the continuity of the area is required and forced as described in Formaggia et al. (2007); Moura (2007), an implicit 3D-1D scheme must be applied. That is the case when using real geometries coming from medical data, since they always have some curvature.

3.3 Other boundary conditions

Different absorbing boundary conditions can be obtained by imposing the absorbing boundary condition of the 1D outflow point, $W_2(Q, \bar{p}) = 0$, directly on the 3D FSI outflow section (Janela et al., 2010b; Nobile and Vergara, 2008). In this case there is no need for solving a 1D problem.

From the expression of $W_2(Q, \bar{p})$ given by (7) and the adopted pressure-area relation (6), condition $W_2(Q, \bar{p}) = 0$ is equivalent to following non linear *formulae*:

$$\sqrt{\frac{8\beta}{\rho A_0}}\left(\bar{p}\frac{A_0}{\beta}+\sqrt{A_0}\right)^2\left(\sqrt{\bar{p}\frac{A_0}{\beta}+\sqrt{A_0}}-A_0^{1/4}\right)=Q. \tag{10}$$

Given the value of the flow rate, Q, the mean pressure, $\bar{p}$, to be prescribed at the outflow 3D FSI section can be easily computed by means of few iterations with the Newton method. From now on, condition (10) will be referred to as non-linear absorbing condition (NAC).

It has been shown that, for physiological values of the Young modulus for the arterial tissue, relation (10) between mean pressure $\bar{p}$ and flow rate Q is almost linear (see Janela et al., 2010b). Having this in mind, a linear boundary condition relating mean pressure and flow rate can be derived considering the first order Taylor approximation of the right hand side of (10) around zero, as described in Janela et al. (2010b):

$$Q \approx \frac{\sqrt{2}A_0^{5/4}}{\sqrt{\rho\beta}}\bar{p}. \tag{11}$$

Expression (11) provides a way of setting the proper resistance at the artificial section of interest, so that the outgoing wave is absorbed. Indeed, a boundary condition of this type, where the mean pressure to be prescribed is linearly computed from the flow rate on that section, can be seen as a coupling between the 3D FSI problem and a simple RL lumped parameters model (see for instance Janela et al. (2010c)). Condition (11) will be referred to as linear absorbing condition (LAC).

In both NAC and LAC conditions, the pressure to be imposed on the 3D FSI changes in time with the flow rate Q. If these conditions are imposed implicitly, we obtain a Robin boundary condition on the 3D FSI artificial section. In this study this complication is avoided using the flow rate at the previous time step to obtain the mean pressure value. This simplification can introduce a phase shift, that should be of the same order of that introduced when using an explicit 3D-1D coupling (Moura, 2007). However, the impact of the explicit algorithms should be further analyzed, the numerical results carried out so far demonstrate the effectiveness of these conditions in both explicit and implicit situations.

Regarding boundary conditions for the solid artificial sections, when taking NAC or LAC boundary conditions, the area can be forced using the same procedure applied to the 3D-1D coupling (Moura, 2007; Formaggia et al., 2007).

Finally, as discussed in Janela et al. (2010b, Remark 6.1), although absorbing boundary conditions can be directly imposed on the 3D FSI model, the coupling with the 1D problem provides physiological information that a strictly absorbing condition does not. In fact, the 1D model allows to account for the global circulation, including for instance upstream and downstream bifurcations.

4 NUMERICAL RESULTS

The non-linear 3D FSI non-Newtonian coupling is solved implicitly through a staggered algorithm using a quasi-Newton method adapted from Fernández and Moubachir (2005), neglecting the shape derivatives.

The time discretization of the structure is carried out through the Newmark mid-point rule (see for instance Moura, 2007). The fluid equations are discretized in time by means of the implicit Euler scheme. The fluid convective and viscous terms are discretized in a semi-implicit way (see Janela et al., 2010a,b). The Arbitrary Lagrangian Eulerian (ALE) formulation is used to account for the evolution of the computational domain, which changes in time due to the FSI coupling (see for instance Nobile, 2001, and references therein). The ALE approach is based on the construction of an appropriate mapping $\mathcal{A}^t : \Omega^0 \to \Omega^t$, $(\hat{\mathbf{x}}, t) \mapsto \mathbf{x} = \mathcal{A}^t(\hat{\mathbf{x}})$, from the reference domain Ω^0, to the current one Ω^t. This technique allows to overcome the mismatch on the coordinate systems between the fluid (Eulerian coordinates) and the solid (Lagrangian coordinates), by simply reformulating the Eulerian time derivative of the fluid momentum equation into the ALE time derivative: $\frac{\partial \mathbf{u}}{\partial t} = \frac{\partial \mathbf{u}}{\partial t}\big|_{\hat{\mathbf{x}}} - (\mathbf{w}\cdot\nabla)\mathbf{u}$, with $\mathbf{w} = \frac{\partial \mathcal{A}^t}{\partial t} \circ (\mathcal{A}^t)^{-1}$ the domain or mesh velocity in the current configuration Ω^t. In particular $\mathcal{A}^t := \mathbf{I}_{\Omega^0} + \boldsymbol{\eta}^f$, where $\boldsymbol{\eta}^f = Ext(\boldsymbol{\eta}|_{\Gamma_w^0})$, being Ext an arbitrary extension of the solid displacement $\boldsymbol{\eta}$ over the fluid reference domain Ω^0, which in this work is the harmonic extension of the fluid domain, imposed through condition (3). We remark that the ALE formulation is fundamental at the discrete level, beacuse it allows to follow the evolution of quantities associated to the moving mesh nodes that were at a different place at the previous time step. However, it is not essential at the continuous level, since in the continuous case the Eulerian time derivative is well defined in all the domain Ω^t, and the problem formulation (1)-(2)-(3)-(4) is thus transparent.

The fluid space discretization is carried out by means of a P1-P1 stabilized streamline diffusion finite element method (Hansbo and Szepessy, 1990), and the structure is approximated with P1 finite elements.

The 3D FSI-1D coupling is performed through a staggered algorithm, subiterating between the 3D FSI and 1D sub-problems (Moura, 2007). The 1D problem is solved by means of the Lax-Wendroff finite element method (Formaggia and Veneziani, 2003). It consists of an explicit time discretization algorithm, hence there is a CFL condition to be verified, making the time step of the 1D problem smaller than the time step of the 3D FSI one. Since the 3D FSI algorithm has a high computational cost, two different time steps are considered for each sub-problem, being the 1D model advanced with constant boundary conditions until the 3D time step is reached (Moura, 2007; Janela et al., 2010b).

4.1 An academic test case: the cylinder

For comparison purposes, the first numerical test consists of a 3D cylinder with $5cm$ length. The lumen radius is $0.5cm$, and wall thickness $0.1cm$. The fluid density is $\rho = 1g/cm^3$, while the structure parameters are: density $\rho_w = 1.2g/cm^3$, Poisson ratio $\xi = 0.3$, and Young modulus $E = 3 \times 10^6 dyne/cm^2$. A pressure of $1.3332 \times 10^4 dyne/cm^2$ ($10mmHg$), during $5 \times 10^{-3}s$ is imposed at the 3D fluid inlet. The vessel wall is considered clamped at inflow, and free to move radially at outflow.

Three different test cases are studied, corresponding to the three different boundary conditions described above. In the case of the 3D FSI - 1D coupling, the 1D model consists of a single tube with the same properties of the 3D FSI model, and a constant viscosity of $\nu = 0.04\ Poi$. The 3D time step is $10^{-3}\ s$, while the 1D time step is $10^{-5}\ s$.

From the numerical results, the differences in the 3D FSI non-Newtonian solutions obtained with the NAC and LAC outflow conditions were negligible (Janela et al., 2010b). Thus, only the results for the LAC absorbing condition are reported.

In Figure 2 (Janela et al., 2010b) are plotted errors in the cross sectional area induced by each set of boundary conditions, with respect to the reference solution considered that of a 3D FSI cylinder with $10cm$ length. The standard solution is that obtained in the $5cm$ cylinder using a standard zero traction boundary condition at the outlet. Figure 3 (Janela et al., 2010b) displays the pressure distribution, as well as the deformation of the domain, amplified by a factor of 10, on the 3D FSI region for the three test cases. From the results, it is clear that both the 3D-1D coupling and LAC conditions absorb the pulse wave of the 3D FSI problem, while the standard boundary condition leads to expected unphysiological pressure wave reflections.

4.2 A realistic test case: the carotid bifurcation

In order to show that the techniques here presented can be applied to any real geometry coming from medical data, an anatomically 3D realistic compliant model of a human carotid bifurcation is considered (Janela et al., 2010b). The physical properties of the problem, as well as the inflow data and time discretization, are the same as in the previous section, with the exception that here the wall thickness is $0.075cm$.

Again, three test cases are considered: standard, LAC condition, and 3D-1D coupling. The later consists of coupling each downstream section of the bifurcation with a 1D single tube of $5cm$ length and radius equal to the 3D radius at which they are coupled. The remaining 1D properties remain as before. At the 3D outflow section the continuity of the area is imposed.

Although no quantitative comparisons can be made in this case, since we do not have a

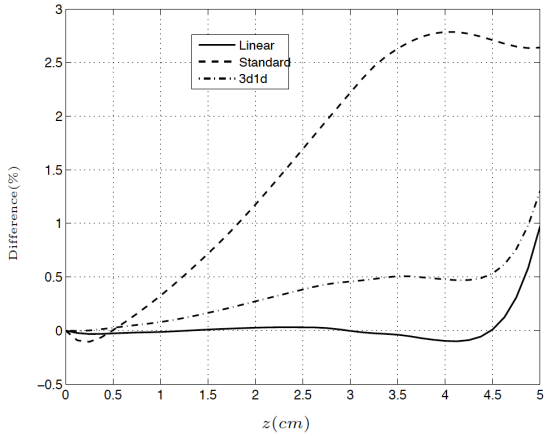

Figure 2: Relative error of the computed cross-sectional area for the LAC, Standard and 3D-1D outflow conditions, with respect to the reference solution in the longer tube

reference solution, Figure 4 demonstrates that both LAC and 3D-1D coupling strategies work very well in absorbing the pressure wave outgoing the 3D model, in accordance to the results presented in the previous section. We can hence conclude that the boundary conditions here presented can be effectively applied in realistic numerical simulations of medical interest.

5 CONCLUSIONS

Different absorbing boundary conditions were presented for a 3D FSI non-Newtonian model for blood flow in arteries, including the coupling of the 3D FSI problem with a 1D model, as well as absorbing boundary conditions to be imposed directly on the 3D FSI outflow section. The simpler boundary conditions, without the coupling with the 1D, proved to effectively absorb the outgoing pressure wave of the 3D FSI model, even when using real patient-specific geometries. Whence, we conclude that the 3D-1D coupling should only be used when a wider arterial network has to be incorporated in the simulations. When the goal is strictly to eliminate the spurious reflections, the absorbing LAC or NAC conditions are efficient and simpler to implement, even in already existing CFD codes.

REFERENCES

Alastruey J., Parker K., Peiró J., Byrd S., and Sherwin S. Modelling the circle of Willis to assess the effects of anatomical variations and occlusions on cerebral flows. *Journal of Biomechanics*, 40(8):1794–1805, 2007.

Chien S., Usami S., Dellenback R.J., and Gregersen M.I. Shear-dependent deformation of erythrocytes in rheology of human blood. *American Journal of Physiology*, 219:136–142, 1970.

Ciarlet P. *Mathematical Elasticity. Vol. 1: Three-Dimensional Elasticity*. Elsevier, 2004.

Fernández M. and Moubachir M. A Newton method using exact Jacobian for solving fluid-structure coupling. *Computers & Structures*, 83(2-3):127–142, 2005.

Formaggia L., Moura A., and Nobile F. On the stability of the coupling of 3D and 1D fluid-structure interaction models for blood flow simulations. *Math. Modell. Num. Anal. (M2AN)*, 41(4):743–769, 2007.

Formaggia L., Quarteroni A., and Veneziani A., editors. *Cardiovascular Mathematics: Mod-*

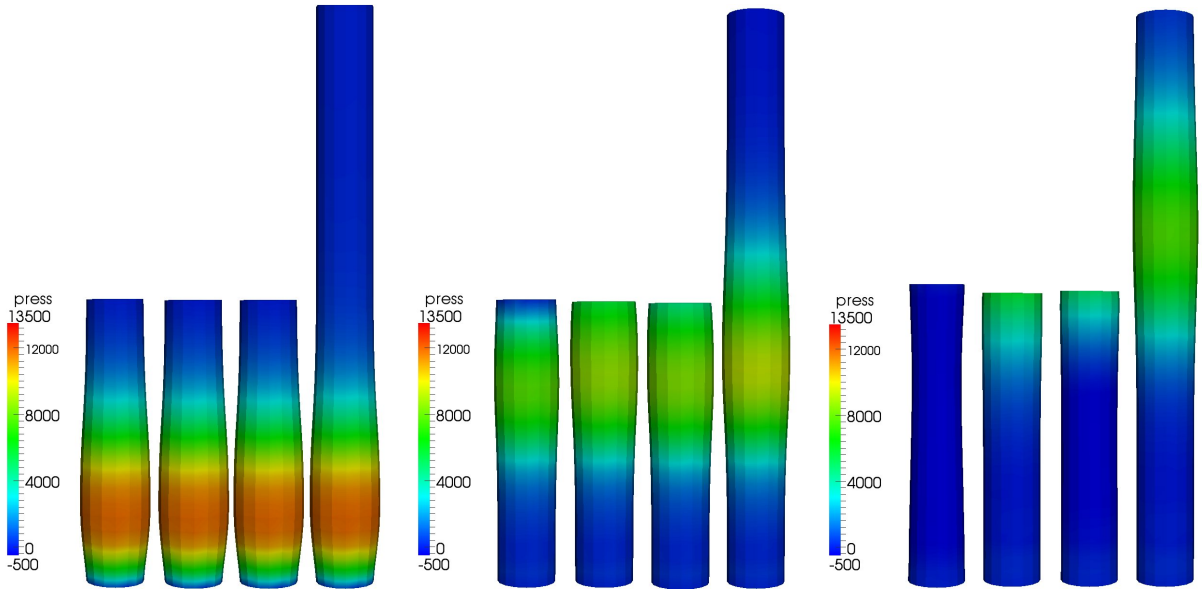

Figure 3: 3D representation of the pressure distribution and computational domain at times $t = 0.005\ s$ (left), $t = 0.01\ s$ (center), and $t = 0.015\ s$ (right). For each time step, from left to right: standard condition; LAC condition; 3D-1D coupling; reference solution.

elling and simulation of the circulatory system. Springer-Verlag Italia, 2009.

Formaggia L. and Veneziani A. Reduced and multiscale models for the human cardiovascular system. *Lecture notes VKI Lecture Series 2003-07, Brussels*, 2003.

Hansbo P. and Szepessy A. A velocity-pressure streamline diffusion finite element method for the incompressible Navier-Stokes equations. *Comput. Methods Appl. Mech. Engrg*, 84(2):175–192, 1990.

Heywood J., Rannacher R., and Turek S. Artificial boundaries and flux and pressure conditions for the incompressible Navier-Stokes equations. *Int. J. Num. Meth. Fluids*, 22:325–352, 1996.

Janela J., Moura A., and Sequeira A. A 3D non-Newtonian fluid-structure interaction model for blood flow in arteries. *J. Comput. Appl. Math.*, 234(9):2783–2791, 2010a.

Janela J., Moura A., and Sequeira A. Absorbing boundary conditions for a 3d non-newtonian fluid-structure interaction model for blood flow in arteries. *ijes*, 2010b. In press.

Janela J., Moura A., and Sequeira A. Towards a geometrical multiscale approach for non-Newtonian blood flow simulations. In *Advances in Mathematical Fluid Mechanics*, pages 295–310. Springer, Berlin, 2010c.

Moura A. *The geometrical multiscale modelling of the cardiovascular system: coupling 3D and 1D models*. Ph.D. thesis, Politecnico di Milano, 2007.

Nobile F. *Numerical approximation of fluid-structure interaction problems with application to haemodynamics*. Ph.D. thesis, Ecole Politechnique Federale de Lausanne, 2001.

Nobile F. and Vergara C. An effective fluid-structure interaction formulation for vascular dynamics by generalized Robin conditions. *SIAM Journal of Scientific Computing*, 30(2):731–763, 2008.

Robertson A., Sequeira A., and Kameneva M. Hemorheology. In G.P. Galdi, R. Rannacher, A. Robertson, and S. Turek, editors, *Haemodynamical Flows: Modelling Analysis and Simulation*, volume 37 of *Oberwolfach Seminars*, pages 63–120. Birkhauser, 2008.

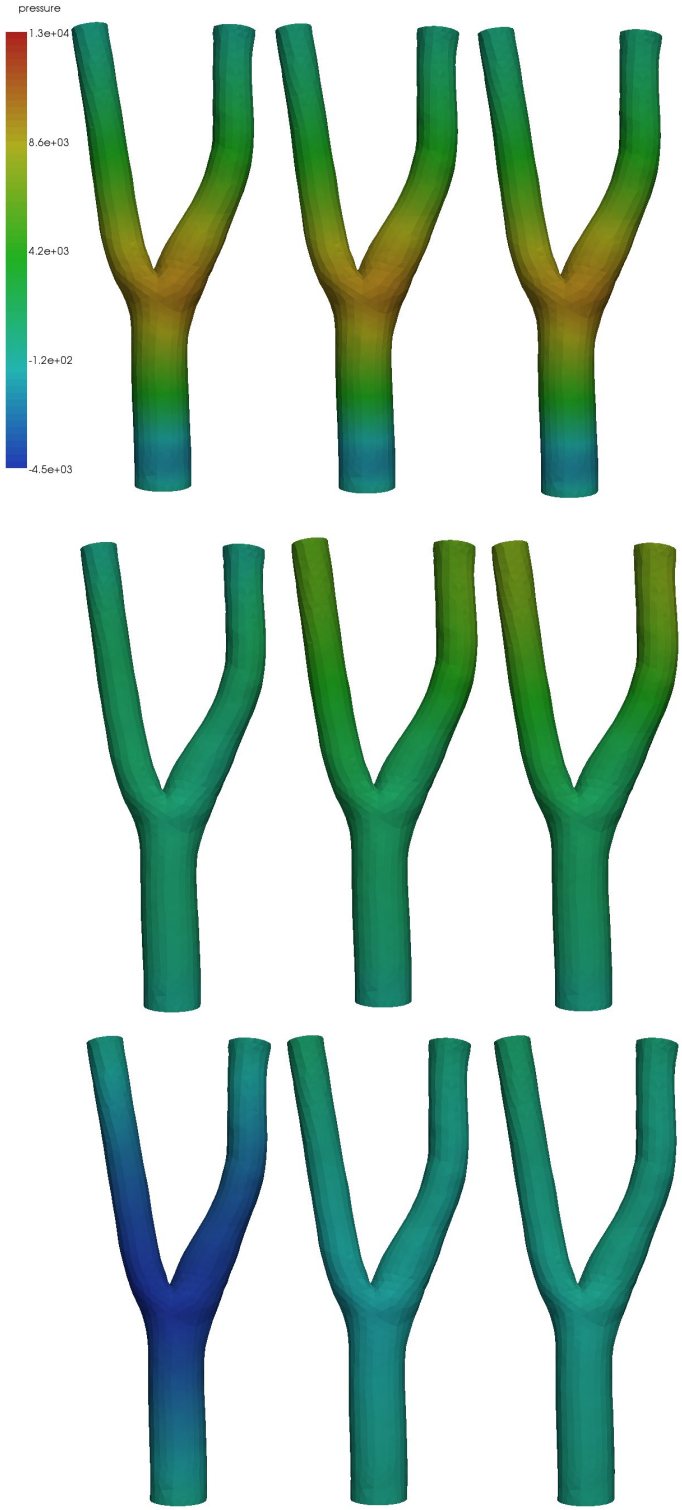

Figure 4: 3D representation of the pressure distribution in a carotid bifurcation, at times $t = 0.007$ (left), $t = 0.014$ (center), and $t = 0.021$ (right), for the standard (left), 3D-1D coupling (center) and LAC (right) test cases.